

# Revisiting Impurity Induced In-gap Bound States In Unconventional Superconductors

Junkang Huang<sup>1,2</sup>, Z. D. Wang<sup>3,4,\*</sup> and Tao Zhou<sup>1,2†</sup>

<sup>1</sup>Guangdong Provincial Key Laboratory of Quantum Engineering and Quantum Materials,  
School of Physics, South China Normal University, Guangzhou 510006, China

<sup>2</sup>Guangdong-Hong Kong Joint Laboratory of Quantum Matter,  
Frontier Research Institute for Physics, South China Normal University, Guangzhou 510006, China

<sup>3</sup>HK Institute of Quantum Science & Technology and Department of Physics,  
The University of Hong Kong, Pokfulam Road, Hong Kong, China

<sup>4</sup>Hong Kong Branch for Quantum Science Center of Guangdong-Hong  
Kong-Macau Great Bay Area, 3 Binlang Road, Shenzhen, China

This study revisits the effects of single impurity scattering in unconventional superconductors, with a specific emphasis on intralayer  $d$ -wave pairing and interlayer  $s$ -wave pairing. We reveal that in the context of a square lattice near half-filling doping, there exists an intrinsic connection between the  $d$ -wave pairing symmetry and the appearance of mid-gap states. This relationship is determined by the  $C_4$  rotational symmetry of both the  $d$ -wave gap amplitude and the square lattice itself. Furthermore, we identify an intrinsic link between the in-gap states and the sign change of the order parameter. In systems with interlayer pairing, strong resonant peaks are observed, despite the absence of sign-reversal characteristics in the pairing order parameter. By utilizing the  $T$ -matrix approach, we elucidate the mechanisms underlying these impurity-induced states. Our theoretical framework is pertinent to the analysis of newly discovered nickel-based high-temperature superconductors, providing a powerful tool for distinguishing their pairing properties. The results of this study shed light on the complex interplay between pairing symmetries and impurity effects in unconventional superconductors, paving the way for future investigations into the unique properties of these emerging materials.

## I. INTRODUCTION

The single impurity effect has been extensively studied in unconventional superconducting systems, including cuprate high-temperature superconductors [1, 2], iron-based superconductors [3–7], as well as other superconducting systems [8–19]. These studies have been facilitated by theoretical explorations and experimental observations through local density of states (LDOS) spectra and scanning tunneling microscopy (STM) measurements.

In the case of cuprate high-temperature superconductors with  $d$ -wave pairing symmetry, a significant finding is the emergence of the mid-gap state induced by a single impurity [1, 2]. The presence of the mid-gap state is attributed to the process of consecutive Andreev reflections [20]. For iron-based superconductors, it has been proposed that impurity effects can serve as a probe for the pairing symmetry, with impurity-induced in-gap states potentially confirming the sign-reversing nature of the superconducting gap across different Fermi surface pockets [3–7].

Theoretically, the impurity effects in unconventional superconducting systems can be analyzed using the  $T$ -matrix method, which suggests that in-gap states are associated with singularities in the  $T$ -matrix denominator [2]. However, the precise relationship between the mid-gap state and  $d$ -wave pairing symmetry within the

$T$ -matrix framework remains to be in-depth explored. In particular, the link between in-gap states and the sign change of the order parameter is not clearly established, indicating a need for further research to clarify these interactions and their impact on system behavior.

Recently, the bilayer nickel-based superconducting material  $\text{La}_3\text{Ni}_2\text{O}_7$  has emerged as a novel high-temperature superconductor, garnering significant research interest [21–24]. The pairing symmetry in this compound remains an open question, with both  $s_{\pm}$  and  $d$ -wave pairing symmetries being proposed [25]. Additionally, several researchers have proposed that nickel-based high-temperature superconducting materials may exhibit dominant interlayer pairing characteristics [26–34]. Therefore, expanding the investigation of single impurity scattering effects to systems dominated by interlayer pairing could be instrumental in elucidating the pairing symmetry of nickel-based superconductors.

In this paper, we revisit the single impurity scattering effects in high-temperature superconducting materials using the  $T$ -matrix method. We consider two scenarios: intralayer pairing and interlayer pairing. For high-temperature superconductors with intralayer pairing, we elucidate why the cuprates with the  $d$ -wave pairing invariably leads to impurity-induced mid-gap states and establish the intrinsic connection between the sign change of the order parameter and the emergence of in-gap states. For  $s$ -wave superconductors with interlayer pairing, our findings indicate that impurities induce strong in-gap resonant states that are not a result of the sign change of the order parameter. We provide a  $T$ -matrix based explanation for this phenomenon.

\* zwang@hku.hk

† tzhou@scnu.edu.cn

The structure of our paper is outlined as follows: In Section II, we introduce the Hamiltonian and the methodologies employed in our study. The impact of impurities in the context of intra-layer pairing is examined in Section II, while Section III is dedicated to discussing the effects of impurities on inter-layer pairing. We conclude with a brief summary of our findings in Section IV.

## II. MODEL AND FORMALISM

Our investigation commences with a multilayer tight-binding model that incorporates superconducting pairing terms, formulated as follows:

$$H = \sum_{\mathbf{k}l} \varepsilon_{\mathbf{k}} c_{\mathbf{k}l}^\dagger c_{\mathbf{k}l} - \sum_{\mathbf{k}} t_{\perp} \left( c_{\mathbf{k}1}^\dagger c_{\mathbf{k}2} + H.c. \right) + H_{\Delta}, \quad (1)$$

where  $\varepsilon_{\mathbf{k}} = -2t(\cos k_x + \cos k_y) - \mu$  with  $t$  being the nearest neighbor hopping constant. Here,  $l$  denotes the layer index,  $\mu$  is the chemical potential, and  $t_{\perp}$  describes the interlayer hopping constant for the bilayer system.

The superconducting pairing term  $H_{\Delta}$  is given by

$$H_{\Delta} = \sum_{\mathbf{k}ll'} \Delta_{\mathbf{k}}^{l,l'} c_{\mathbf{k}l}^\dagger c_{\mathbf{k}l'} + H.c., \quad (2)$$

where  $l = l'$  and  $l \neq l'$  represent the intralayer pairing and interlayer pairing, respectively.

The bare Green's function matrix for a clean system can be obtained through diagonalizing the Hamiltonian matrix, with the elements being defined as

$$G_{0ij}(\mathbf{k}, \omega) = \sum_n \frac{u_{in}(\mathbf{k}) u_{jn}^*(\mathbf{k})}{\omega - E_n(\mathbf{k}) + i\Gamma}, \quad (3)$$

where  $u_{in}(\mathbf{k})$  and  $E_n(\mathbf{k})$  are the eigenvectors and the eigenvalue of the Hamiltonian matrix, respectively.  $\Gamma$  is a small constant.

Considering a single impurity at the site  $(0, 0)$  of layers 1, the  $T$ -matrix can be expressed as [2]

$$T(\omega) = \frac{U}{I - U G_0(\mathbf{r}, \mathbf{r}, \omega)}, \quad (4)$$

where  $I$  is the identity matrix,  $U$  is a diagonal matrix with non-zero elements  $U_{11} = V_{\text{imp}}$  and  $U_{33} = -V_{\text{imp}}$ , and  $G_0(\mathbf{r}, \mathbf{r}', \omega)$  is the Fourier transform of  $G_0(\mathbf{k}, \omega)$  with  $G_0(\mathbf{r}, \mathbf{r}', \omega) = \frac{1}{N} \sum_{\mathbf{k}} G_0(\mathbf{k}, \omega) e^{i\mathbf{k} \cdot (\mathbf{r} - \mathbf{r}')}$ .

The full Green's function in the presence of a single impurity is calculated by:

$$G(\mathbf{r}, \mathbf{r}', \omega) = G_0(\mathbf{r}, \mathbf{r}', \omega) + G_0(\mathbf{r}, 0, \omega) T(\omega) G_0(0, \mathbf{r}', \omega). \quad (5)$$

The LDOS at layer  $l$  and site  $\mathbf{r}$  can be calculated using the full Green's function:

$$\rho_l(\mathbf{r}, \omega) = -\frac{1}{\pi} \text{Im} [G_{ll}(\mathbf{r}, \mathbf{r}, \omega) + G_{l+2, l+2}(\mathbf{r}, \mathbf{r}, -\omega)]. \quad (6)$$

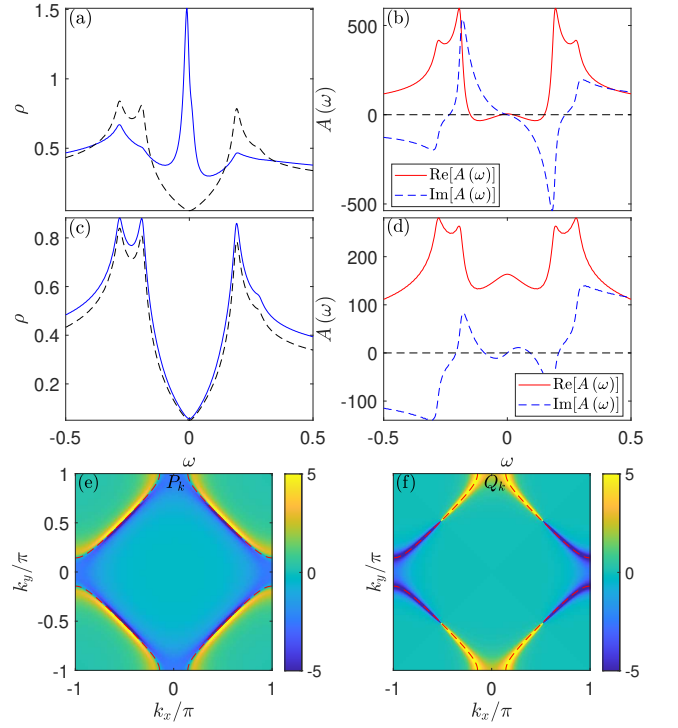


FIG. 1. Solid line: LDOS spectrum at the nearest neighbor site of the impurity site for a  $d_{x^2-y^2}$ -wave pairing scenario. The dashed line represents the bare LDOS spectrum in the absence of the impurity. (b) Real and imaginary components of the function  $A(\omega)$  for the  $d$ -wave pairing symmetry. Panels (c) and (d) correspond to panels (a) and (b), respectively, but for the sign-unchanged pairing with  $\Delta_{\mathbf{k}} = |\Delta_0(\cos k_x - \cos k_y)|/2$ . Panels (e) and (f) display the intensity distribution maps for the functions  $P_{\mathbf{k}}$  and  $Q_{\mathbf{k}}$ , respectively. The dashed lines in panels (e) and (f) indicate the normal state Fermi surface.

In this paper, we set the nearest-neighbor hopping parameter  $t$  as the energy unit with  $t = 1$ . Other parameters are set as  $\Gamma = 0.01$  and  $V_{\text{imp}} = 20$ .

## III. IMPURITY EFFECT WITH THE INTRALAYER PAIRING

We now study the impurity effect with intralayer pairing based on a single-layer model by setting  $l \equiv 1$  and  $t_{\perp} = 0$  in Eq. (1). Initially, we re-exhibit the numerical results for the impurity effect on  $d_{x^2-y^2}$ -wave superconductors, taking  $\Delta_{\mathbf{k}} = \Delta_0(\cos k_x - \cos k_y)/2$  with  $\Delta_0 = 0.2$ . The LDOS spectra without the impurity and near an impurity are plotted in Fig. 1(a). As observed, without the impurity, a  $V$ -shaped spectrum is obtained due to the existence of nodal points of the  $d$ -wave pairing symmetry. A sharp mid-gap resonant peak emerges near the Fermi energy in the presence of the impurity. This mid-gap resonant peak can be explained through

the denominator of the  $T$ -matrix,  $A(\omega)$ , with

$$A(\omega) = \text{Det} [I - UG_0(\mathbf{r}, \mathbf{r}, \omega)].$$

The impurity-induced resonant peaks emerge when both the real part and the imaginary part of  $A(\omega)$  are zero at a certain low energy. For the  $d$ -wave pairing symmetry, the real and imaginary parts of  $A(\omega)$  as a function of the energy  $\omega$  are shown in Fig. 1(b). As seen, the imaginary part of  $A(\omega)$  crosses the zero axis at  $\omega = 0$ , and the real part also crosses the zero axis near the Fermi level, leading to the mid-gap resonant peak.

It is widely believed that the mid-gap state presented in Fig. 1(a) arises from the sign change of the  $d$ -wave order parameter. To verify this conclusion numerically, we consider the sign-unchanged order parameter with  $\Delta_{\mathbf{k}} = |\Delta_0(\cos k_x - \cos k_y)/2|$ . It's important to clarify that this specific configuration of the order parameter is not representative of any actual material; rather, it serves as a theoretical construct designed to highlight how the sign change in order parameters influences the impurity effect. The LDOS spectra, both in the absence and presence of an impurity with this order parameter form, are illustrated in Figure 1(c). The corresponding real and imaginary parts of  $A(\omega)$  are displayed in Fig. 1(d). As is seen, although the base LDOS spectrum without the impurity is the same as that of the  $d$ -wave superconductor, the spectrum in the presence of the impurity is significantly different. In this case, no in-gap structure exists. This absence of in-gap structure aligns with the numerical calculations of the denominator of the  $T$ -matrix,  $A(\omega)$ , where the real part of  $A(\omega)$  is significantly far from the zero axis, as seen in Fig. 1(d). These numerical results indicate that the impurity effect is indeed sensitive to the phase of the order parameter and thus can be used to detect the sign change of the order parameter.

To delve deeper into the connections between the in-gap states and the sign-changing of the order parameter, we derive the  $T$ -matrix analytically. Since the spectral function and LDOS spectra are generally small at low energies, the imaginary part of  $A(\omega)$  is also generally small within the superconducting gap. As a result, the impurity-induced low-energy features are mainly determined by the real part of  $A(\omega)$ . The real part of  $A(\omega)$  at zero energy is expressed as:

$$A(0) = V_{\text{imp}}^2 \left[ \left( \sum_{\mathbf{k}} P_{\mathbf{k}} \right)^2 + \left( \sum_{\mathbf{k}} Q_{\mathbf{k}} \right)^2 \right], \quad (7)$$

where  $P_{\mathbf{k}}$  and  $Q_{\mathbf{k}}$  can be written as:

$$P_{\mathbf{k}} = \frac{\varepsilon_{\mathbf{k}}}{\varepsilon_{\mathbf{k}}^2 + \Delta_{\mathbf{k}}^2}, \quad (8)$$

$$Q_{\mathbf{k}} = \frac{\Delta_{\mathbf{k}}}{\varepsilon_{\mathbf{k}}^2 + \Delta_{\mathbf{k}}^2}. \quad (9)$$

$P_{\mathbf{k}}$  and  $Q_{\mathbf{k}}$  are large only in the vicinity of the normal state Fermi surface and should rapidly drop to nearly

zero away from the Fermi surface. The intensity plots of  $P_{\mathbf{k}}$  and  $Q_{\mathbf{k}}$  are presented in Figs. 1(e) and 1(f), respectively.  $P_{\mathbf{k}}$  is positive for the hole region and negative for the electron region, and it changes sign as it crosses the Fermi surface. For a half-filled system, the summation of  $P_{\mathbf{k}}$  over the entire Brillouin zone results in positive and negative values canceling each other out, generally leading to a zero value. For cuprate superconductors, which are near half-filled, the summation of  $P(\mathbf{k})$  results in a small value. On the other hand, for the  $d$ -wave pairing symmetry, both the normal state energy bands and the gap magnitudes have the  $C_4$  rotational symmetry with  $\varepsilon(k_x, k_y) \equiv \varepsilon(-k_y, k_x)$  and  $\Delta(k_x, k_y) \equiv -\Delta(-k_y, k_x)$ , thus the summation of  $Q_{\mathbf{k}}$  is exactly zero. Consequently,  $A(\omega)$  is nearly zero at the Fermi level for cuprate high- $T_c$  superconductors, leading to strong mid-gap resonant peaks in the LDOS spectrum near an impurity.

We now investigate whether an inevitable connection exists between the sign change of the order parameter along the normal state Fermi surface and in-gap states. We introduce an additional  $s$ -wave component into the  $d_{x^2-y^2}$ -wave pairing function, defined as  $\Delta_{\mathbf{k}} = \Delta_s + \Delta_d(\cos k_x - \cos k_y)/2$ , with  $\Delta_d = 0.2$ . This component breaks the  $C_4$  symmetry of the gap magnitudes. As  $\Delta_s$  increases, the gap nodes shift from the diagonal direction towards the Brillouin zone boundary. Consequently,  $\sum_{\mathbf{k}} Q(\mathbf{k})$  increases as  $\Delta_s$  increases. A critical  $s$ -wave magnitude  $\Delta_s^c$  can be defined, where the gap nodes shift exactly onto the Brillouin zone boundary. When  $\Delta_s$  equals or exceeds  $\Delta_s^c$ , the sign of the order parameter  $\Delta_{\mathbf{k}}$  does not change along the entire normal state Fermi surface.  $\Delta_s^c$  depends on the chemical potential and is expressed as  $\Delta_s^c = \Delta_d(1 - |\mu/4|)$  [35].

We consider two different chemical potentials,  $\mu = 0.2$  and  $\mu = 2$ , with corresponding critical  $s$ -wave magnitudes of  $\Delta_s^c = 0.19$  and  $\Delta_s^c = 0.1$ , respectively. The LDOS spectra for different values of  $\Delta_s$  are shown in Figs. 2(a) and 2(b), and the corresponding real parts of the denominator of the  $T$ -matrix,  $\text{Re} A(\omega)$ , are presented in Figs. 2(c) and 2(d). For the case of  $\mu = 0.2$ , as seen from Fig. 2(a), the presence of the  $s$ -wave component causes the mid-gap peak to split, with the intensity decreasing as  $\Delta_s$  increases. The in-gap features disappear completely when  $\Delta_s$  reaches the critical value (0.19). For the case of  $\mu = 2$ , weak in-gap peaks appear at finite energy even in the absence of the  $s$ -wave component. Similarly, the in-gap features disappear completely when  $\Delta_s$  reaches its corresponding critical value (0.1).

The in-gap features presented in Figs. 2(a) and 2(b) are consistent with the denominator of the  $T$ -matrix,  $\text{Re} A(\omega)$ , shown in Figs. 2(c) and 2(d). Specifically, when  $\Delta_s$  is smaller than  $\Delta_s^c$ ,  $\text{Re} A(\omega)$  concaves down and has local minimal points at low energies, resulting in the in-gap feature. As  $\Delta_s$  reaches the critical value, the curve of  $\text{Re} A(\omega)$  concaves up, and the in-gap features disappear completely.

Two key insights arise from these numerical results. First, the intensity of the resonant mid-gap peak de-

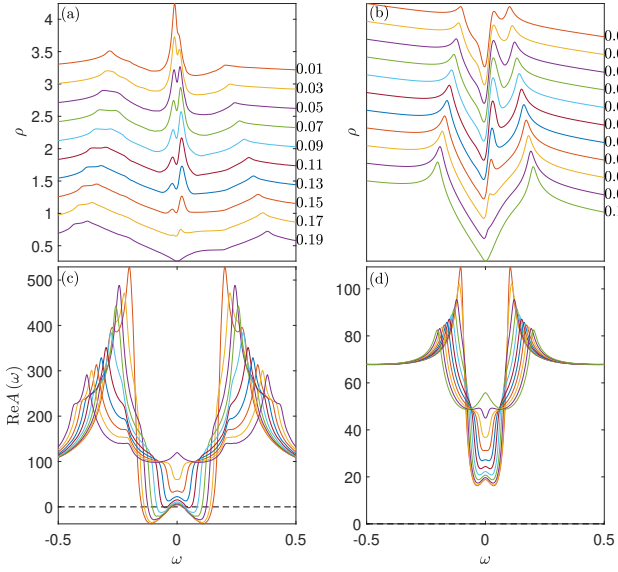


FIG. 2. (a) LDOS spectra at the nearest neighbor site of the impurity for the  $s + d_{x^2-y^2}$  wave model, with a chemical potential of  $\mu = 0.2$  and pairing defined as  $\Delta_{\mathbf{k}} = \Delta_s + \Delta(\cos k_x - \cos k_y)/2$ . The parameter  $\Delta_s$  increases from 0.01 to 0.19 from top to bottom. (b) Similar to panel (a), but for a chemical potential of  $\mu = 2$ .  $\Delta_s$  increasing from 0.01 to 0.1. Panels (c) and (d) show the real parts of the function  $A(\omega)$  corresponding to panels (a) and (b), respectively.

creases with increasing chemical potential. Second, there is a clear intrinsic relationship between the in-gap states and the sign reversal of the superconducting order parameter along the Fermi surface.

The absence of a strong resonant mid-gap peak for  $\mu = 2$  can be understood by analyzing the function  $P_{\mathbf{k}}$ . When the chemical potential is large, as with  $\mu = 2$ , the system is heavily electron-doped, and the summation of  $P_{\mathbf{k}}$  over the entire Brillouin zone results in a relatively larger negative value. Consequently, the resonant condition  $A(\omega) = 0$  is not satisfied, and weaker in-gap peaks emerge at the position where  $\text{Re } A(\omega)$  is minimal, as seen from Fig. 2(d).

The crucial connection between the in-gap states and the sign-changing of the order parameter is further confirmed and understood by exploring the denominator of the  $T$ -matrix as  $\Delta_s$  crosses the critical value. We present the numerical results of  $\text{Re } A(\omega)$  with  $\Delta_s = 0.9\Delta_s^c$  and  $\Delta_s = \Delta_s^c$  for chemical potentials ranging from 0 to 2 in Figs. 3(a) and 3(b), respectively. As is seen, when  $\Delta_s$  is slightly below the critical value, the curve concaves down at low energies for all chemical potentials considered. Instead, as  $\Delta_s$  increases to the critical value, all curves turn to concave up at low energies. When  $\Delta_s$  is smaller than  $\Delta_s^c$ , the normal state Fermi surface has nodal points, and the order parameter changes sign crossing the nodal points. In this case, the summation of  $Q_{\mathbf{k}}$  along the Fermi surface reduces because some positive and negative values of  $Q_{\mathbf{k}}$  cancel each other out, leading to the concaving

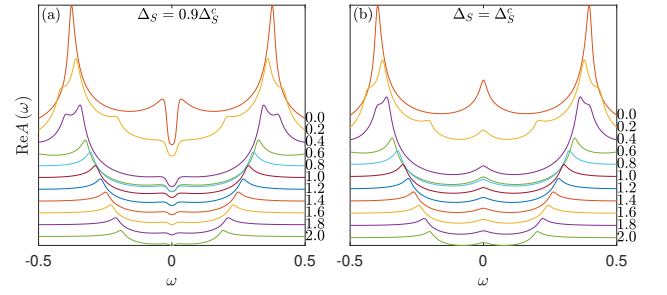


FIG. 3. (a) The real part of the function  $A(\omega)$  as a function of  $\omega$  for the  $s + d_{x^2-y^2}$  wave model with the  $s$ -wave component  $\Delta_s = 0.9\Delta_s^c$ . The chemical potential  $\mu$  increases from 0 to 2 from top to bottom. (b) Similar to panel (a) but for a different  $s$ -wave component  $\Delta_s = \Delta_s^c$ .

down behavior for  $\text{Re } A(\omega = 0)$ . Such concaving down behavior further leads to the in-gap features.

#### IV. IMPURITY EFFECT WITH THE INTERLAYER PAIRING

We now turn our attention to the bilayer system with strong interlayer hopping by setting  $l = 1, 2$  and  $t_{\perp} = 1.5$  in Eq. (1). Consequently, the normal state Fermi surface splits into two pockets defined by  $\varepsilon_{\mathbf{k}} \pm t_{\perp} = 0$ . The superconducting order parameters in Eq. (2) are set as the  $s$ -wave inter-layer pairing with  $\Delta_{\mathbf{k}}^{1,2} = \Delta_{\mathbf{k}}^{2,1} = \Delta_{\perp}$ . Similar to the case of intralayer pairing, we define the denominator of the  $T$ -matrix,  $A(\omega)$ , with the real part of  $A(\omega)$  at zero energy being expressed as:

$$A(0) = V_{\text{imp}}^2 \left[ \left( \sum_{\mathbf{k}} P'_{\mathbf{k}} \right)^2 + \left( \sum_{\mathbf{k}} Q'_{\mathbf{k}} \right)^2 \right], \quad (10)$$

$$P'_{\mathbf{k}} = \frac{\varepsilon_{\mathbf{k}} (\varepsilon_{\mathbf{k}}^2 - t_{\perp}^2 + \Delta_{\perp}^2)}{\text{Det}[H(\mathbf{k})]}, \quad (11)$$

$$Q'_{\mathbf{k}} = \frac{2\varepsilon_{\mathbf{k}} t_{\perp} \Delta_{\perp}}{\text{Det}[H(\mathbf{k})]}, \quad (12)$$

$$\text{Det}[H(\mathbf{k})] = t_{\perp}^4 + 2t_{\perp}^2 (\Delta_{\perp}^2 - \varepsilon_{\mathbf{k}}^2) + (\Delta_{\perp}^2 + \varepsilon_{\mathbf{k}}^2)^2 \quad (13)$$

$P'_{\mathbf{k}}$  and  $Q'_{\mathbf{k}}$  share some similar properties with  $P_{\mathbf{k}}$  and  $Q_{\mathbf{k}}$ , i.e.,  $\text{Det}[H(\mathbf{k})]$  reaches its minimum value as  $\varepsilon_{\mathbf{k}}^2 = t_{\perp}^2$ , thus both  $P'_{\mathbf{k}}$  and  $Q'_{\mathbf{k}}$  are large along the normal state Fermi surface and tend to zero away from the Fermi surface.  $P'_{\mathbf{k}}$  changes sign as it crosses the Fermi surface, and the summation of  $P'_{\mathbf{k}}$  over the entire Brillouin zone results in a very small value. However, unlike  $Q_{\mathbf{k}}$ , where the sign is determined by the gap function [Eq. (9)], the sign of  $Q'_{\mathbf{k}}$  is determined by  $\varepsilon_{\mathbf{k}} \Delta_{\perp}$ . Here, the pairing function  $\Delta_{\perp}$  is a constant value, while  $\varepsilon_{\mathbf{k}}$  changes sign for the two Fermi pockets. As a result, the summation of  $Q'_{\mathbf{k}}$  over the entire Brillouin zone is generally small. Therefore, for superconductors with interlayer pairing,

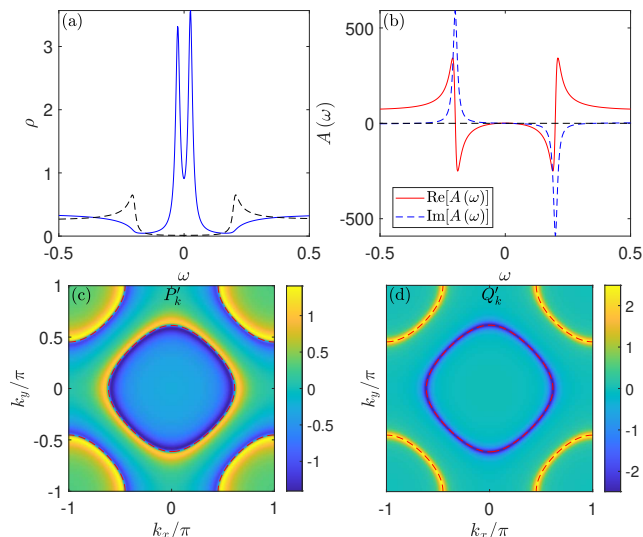


FIG. 4. (a) Solid line: LDOS spectrum at the nearest neighbor site of the impurity site for the interlayer pairing scenario. The dashed line represents the bare LDOS spectrum in the absence of the impurity. (b) Real and imaginary components of the function  $A(\omega)$  for the interlayer pairing. Panels (c) and (d) display the intensity distribution maps for the functions  $P'_k$  and  $Q'_k$ , respectively. The dashed lines in panels (c) and (d) indicate the normal state Fermi surface.

our analytical calculation indicates that in-gap resonant peaks generally exist.

This conclusion can be confirmed numerically. We present the numerical results of the LDOS spectra with  $\Delta_{\perp} = 0.2$  and  $\mu = 0.2$  in Fig. 4(a). The real and imaginary parts of  $A(\omega)$  as a function of  $\omega$  are plotted in Fig. 4(b). As is seen, without the impurity, the LDOS spectrum is 'U' shaped, indicating that the system is fully gapped. In the presence of an impurity, two sharp resonant peaks emerge, with the peak position lying symmetrically about the Fermi energy. The existence of the resonant peaks is consistent with the pole condition of the  $T$ -matrix. As seen in Fig. 4(b), both the real part and the imaginary part of  $A(\omega)$  tend to zero at low energies. This result is consistent with the analytical formulas of  $A(\omega)$  presented in Eqs. (10-13).

Recently, the bilayer nickelate superconductor  $\text{La}_3\text{Ni}_2\text{O}_7$  has garnered significant attention from researchers. The pairing symmetry for this material remains an open question. For intralayer dominant pairing, several possible pairing symmetries have been proposed theoretically, including the  $s_{\pm}$  pairing symmetry and  $d$ -wave pairing symmetry [25]. It has also been proposed that the dominant interlayer pairing accounts for the superconductivity [26–34]. Our impurity scattering theory may be directly applied to

nickelate superconductors and used to probe the pairing function. Based on the numerical results presented in Sec. III, we infer that if intra-layer  $d$ -wave pairing is predominant, strong mid-gap states should be present. Conversely, if intra-layer  $s_{\pm}$ -wave pairing is dominant, the positive and negative contributions to  $Q_{\mathbf{k}}$  cannot be completely cancelled out, leading to the presence of weaker in-gap states. The numerical results for these two pairing symmetries, which are in agreement with our conclusions, have been detailed in Ref. [12].

We also started from the model describing the  $\text{La}_3\text{Ni}_2\text{O}_7$  material and considered the interlayer pairing. The impurity effect was studied theoretically, and the results are similar to those presented in Fig. 4, namely, sharp resonant peaks exist at low energies inside the superconducting gap [35]. Therefore, we here propose that the impurity-induced in-gap states can be used as a powerful tool to probe the pairing symmetry of  $\text{La}_3\text{Ni}_2\text{O}_7$  superconductors.

## V. SUMMARY

We have undertaken a detailed exploration of single impurity scattering in unconventional superconductors, with a focus on intralayer  $d$ -wave and interlayer  $s$ -wave pairing. In the case of intralayer  $d$ -wave pairing near half-filling doping in a square lattice, an inherent link between the  $d$ -wave pairing symmetry and the appearance of mid-gap states is revealed. This connection is firmly rooted in the  $C_4$  rotational symmetry of both the  $d$ -wave gap amplitude and the square lattice. Additionally, a strong interplay between in-gap states and the sign change of the order parameter is established.

For interlayer pairing systems, despite the absence of sign-reversing features in the pairing order parameter, prominent resonant peaks are revealed. By employing the  $T$ -matrix approach, the underlying mechanisms responsible for these impurity-induced states are successfully explained. This theoretical framework proves highly applicable to the analysis of newly discovered nickel-based high-temperature superconductors and serves as a valuable means for distinguishing their pairing properties.

Overall, this study illuminates the intricate relationship between pairing symmetries and impurity effects in unconventional superconductors, laying a solid foundation for future research on the unique characteristics of these materials and offering a potential method for probing the pairing symmetry of nickel-based superconductors like  $\text{La}_3\text{Ni}_2\text{O}_7$ .

This work was supported by the NSFC under the Grant No.12074130.

[1] E. W. Hudson, S. H. Pan, A. K. Gupta, K.-W. Ng, and J. C. Davis, Atomic-scale quasi-particle scattering reso-

nances in  $\text{Bi}_2\text{Sr}_2\text{CaCu}_2\text{O}_{8+\delta}$ , *Science* **285**, 88 (1999).

- [2] A. V. Balatsky, I. Vekhter, and J.-X. Zhu, Impurity-induced states in conventional and unconventional superconductors, *Rev. Mod. Phys.* **78**, 373 (2006).
- [3] T. Zhou, H. Huang, Y. Gao, J.-X. Zhu, and C. S. Ting, Quasiparticle states around a nonmagnetic impurity in electron-doped iron-based superconductors with spin-density-wave order, *Phys. Rev. B* **83**, 214502 (2011).
- [4] Y. Gao, Y. Yu, T. Zhou, H. Huang, and Q.-H. Wang, In-gap bound states induced by a single nonmagnetic impurity in sign-preserving  $s$ -wave superconductors with incipient bands, *Phys. Rev. B* **96**, 220507 (2017).
- [5] W.-F. Tsai, Y.-Y. Zhang, C. Fang, and J. Hu, Impurity-induced bound states in iron-based superconductors with  $s$ -wave  $\cos k_x \cdot \cos k_y$  pairing symmetry, *Phys. Rev. B* **80**, 064513 (2009).
- [6] Y. Gao, Y. Yu, T. Zhou, H. Huang, and Q.-H. Wang, Hidden sign-changing  $s$ -wave superconductivity in monolayer fese, *Phys. Rev. B* **94**, 144512 (2016).
- [7] D. Zhang, Nonmagnetic impurity resonances as a signature of sign-reversal pairing in feas-based superconductors, *Phys. Rev. Lett.* **103**, 186402 (2009).
- [8] T. O. Wehling, H. P. Dahal, A. I. Lichtenstein, and A. V. Balatsky, Local impurity effects in superconducting graphene, *Phys. Rev. B* **78**, 035414 (2008).
- [9] Y.-Q. Li and T. Zhou, Impurity effect as a probe for the pairing symmetry of graphene-based superconductors, *Front. Phys.* **16**, 10.1007/s11467-021-1056-y (2021).
- [10] J. Liu and T. Zhou, Probing the pairing symmetry in kagome superconductors based on the single-particle spectrum, *Phys. Rev. B* **109**, 054504 (2024).
- [11] S. C. Holbæk, M. H. Christensen, A. Kreisel, and B. M. Andersen, Unconventional superconductivity protected from disorder on the kagome lattice, *Phys. Rev. B* **108**, 144508 (2023).
- [12] J. Huang, Z. D. Wang, and T. Zhou, Impurity and vortex states in the bilayer high-temperature superconductor  $\text{La}_3\text{Ni}_2\text{O}_7$ , *Phys. Rev. B* **108**, 174501 (2023).
- [13] T. Zhou, Y. Gao, and Z. D. Wang, Resolving different pairing states in weyl superconductors through the single-particle spectrum, *Phys. Rev. B* **98**, 024515 (2018).
- [14] H. Hu, L. Jiang, H. Pu, Y. Chen, and X.-J. Liu, Universal impurity-induced bound state in topological superfluids, *Phys. Rev. Lett.* **110**, 020401 (2013).
- [15] X.-J. Liu, Impurity probe of topological superfluids in one-dimensional spin-orbit-coupled atomic fermi gases, *Phys. Rev. A* **87**, 013622 (2013).
- [16] J. D. Sau and E. Demler, Bound states at impurities as a probe of topological superconductivity in nanowires, *Phys. Rev. B* **88**, 205402 (2013).
- [17] Y. Nagai, Y. Ota, and M. Machida, Nonmagnetic impurity effects in a three-dimensional topological superconductor: From  $p$ - to  $s$ -wave behaviors, *Phys. Rev. B* **89**, 214506 (2014).
- [18] C. Setty, P. W. Phillips, and A. Narayan, Quasiparticle interference and resonant states in normal and superconducting line nodal semimetals, *Phys. Rev. B* **95**, 140202 (2017).
- [19] M. Wimmer, A. R. Akhmerov, M. V. Medvedeva, J. Tworzydło, and C. W. J. Beenakker, Majorana bound states without vortices in topological superconductors with electrostatic defects, *Phys. Rev. Lett.* **105**, 046803 (2010).
- [20] C.-R. Hu, Midgap surface states as a novel signature for  $d_{x^2-y^2}^2$ -wave superconductivity, *Phys. Rev. Lett.* **72**, 1526 (1994).
- [21] H. Sun, M. Huo, X. Hu, J. Li, Z. Liu, Y. Han, L. Tang, Z. Mao, P. Yang, B. Wang, J. Cheng, D.-X. Yao, G.-M. Zhang, and M. Wang, Signatures of superconductivity near 80K in a nickelate under high pressure, *Nature* **621**, 493 (2023).
- [22] Z. Luo, X. Hu, M. Wang, W. Wú, and D.-X. Yao, Bilayer two-orbital model of  $\text{La}_3\text{Ni}_2\text{O}_7$  under pressure, *Phys. Rev. Lett.* **131**, 126001 (2023).
- [23] E. K. Ko, Y. Yu, Y. Liu, L. Bhatt, J. Li, V. Thampy, C.-T. Kuo, B. Y. Wang, Y. Lee, K. Lee, J.-S. Lee, B. H. Goodge, D. A. Muller, and H. Y. Hwang, Signatures of ambient pressure superconductivity in thin film  $\text{La}_3\text{Ni}_2\text{O}_7$ , *Nature* 10.1038/s41586-024-08525-3 (2024).
- [24] G. Zhou, W. Lv, H. Wang, Z. Nie, Y. Chen, Y. Li, H. Huang, W. Chen, Y. Sun, Q.-K. Xue, and Z. Chen, Ambient-pressure superconductivity onset above 40 K in bilayer nickelate ultrathin films, [arXiv:2412.16622](https://arxiv.org/abs/2412.16622) [[cond-mat.supr-con](https://arxiv.org/abs/2412.16622)].
- [25] M. Wang, H.-H. Wen, T. Wu, D.-X. Yao, and T. Xiang, Normal and superconducting properties of  $\text{La}_3\text{Ni}_2\text{O}_7$ , *Chinese Physics Letters* **41**, 077402 (2024).
- [26] K.-J. Zhou, X. Chen, J. Choi, Z. Jiang, J. Mei, K. Jiang, J. Li, S. Agrestini, M. Garcia-Fernandez, H. Sun, X. Huang, D. Shen, M. Wang, J. Hu, Y. Lu, and D. Feng, *Electronic and magnetic excitations in  $\text{La}_3\text{Ni}_2\text{O}_7$*  (2024).
- [27] T. Xie, M. Huo, X. Ni, F. Shen, X. Huang, H. Sun, H. C. Walker, D. Adroja, D. Yu, B. Shen, L. He, K. Cao, and M. Wang, Strong interlayer magnetic exchange coupling in  $\text{La}_3\text{Ni}_2\text{O}_{7-\delta}$  revealed by inelastic neutron scattering, *Sci. Bull.* **69**, 3221 (2024).
- [28] Y.-f. Yang, G.-M. Zhang, and F.-C. Zhang, Interlayer valence bonds and two-component theory for high- $T_c$  superconductivity of  $\text{La}_3\text{Ni}_2\text{O}_7$  under pressure, *Phys. Rev. B* **108**, L201108 (2023).
- [29] C. Lu, Z. Pan, F. Yang, and C. Wu, Interplay of two  $E_g$  orbitals in superconducting  $\text{La}_3\text{Ni}_2\text{O}_7$  under pressure, *Phys. Rev. B* **110**, 094509 (2024).
- [30] H. Oh and Y.-H. Zhang, Type-II  $t - J$  model and shared superexchange coupling from hund's rule in superconducting  $\text{La}_3\text{Ni}_2\text{O}_7$ , *Phys. Rev. B* **108**, 174511 (2023).
- [31] J. Chen, F. Yang, and W. Li, Orbital-selective superconductivity in the pressurized bilayer nickelate  $\text{La}_3\text{Ni}_2\text{O}_7$ : An infinite projected entangled-pair state study, *Phys. Rev. B* **110**, L041111 (2024).
- [32] C. Lu, Z. Pan, F. Yang, and C. Wu, Interlayer-coupling-driven high-temperature superconductivity in  $\text{La}_3\text{Ni}_2\text{O}_7$  under pressure, *Phys. Rev. Lett.* **132**, 146002 (2024).
- [33] J.-R. Xue and F. Wang, Magnetism and superconductivity in the  $t - J$  model of  $\text{La}_3\text{Ni}_2\text{O}_7$  under multiband gutzwiller approximation, *Chin. Phys. Lett.* **41**, 057403 (2024).
- [34] M. Lu and T. Zhou, Spin excitations in bilayer  $\text{La}_3\text{Ni}_2\text{O}_7$  superconductors with the interlayer pairing, [arXiv:2408.10638](https://arxiv.org/abs/2408.10638) [[cond-mat.supr-con](https://arxiv.org/abs/2408.10638)].
- [35] See supplemental material for revisiting impurity induced in-gap bound states in unconventional superconductors.

# Supplemental Material For Revisiting Impurity Induced In-gap Bound States In Unconventional Superconductors

## S-1. THE CRITICAL $s$ -WAVE COMPONENT

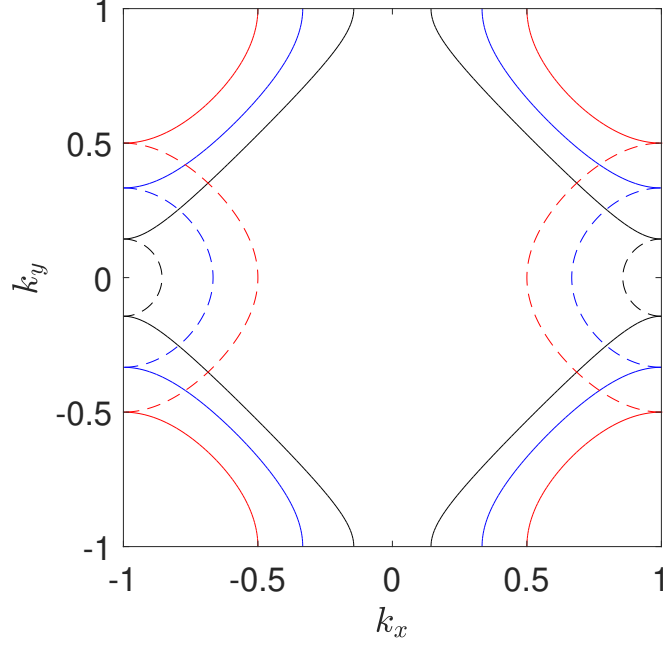


FIG. S1. The solid red, blue, and black lines represent the Fermi surfaces in the normal state for chemical potentials of  $\mu = 2$ ,  $\mu = 1$ , and  $\mu = 0.2$ , respectively. The corresponding dashed red, blue, and black lines depict the nodal lines of the energy gap when  $\Delta_s = \Delta_s^c(\mu)$ .

In the main text, for the  $s + d_{x^2-y^2}$  pairing symmetry, the order parameter is given by  $\Delta_{\mathbf{k}} = \Delta_s + \Delta_d(\cos k_x - \cos k_y)/2$ . In this context, we define the critical  $s$ -wave component  $\Delta_s^c$ , which depends on the chemical potential  $\mu$  according to the equation  $\Delta_s^c(\mu) = \Delta_d(1 - |\mu/4|)$ . At the critical value  $\Delta_s = \Delta_s^c$ , the normal state Fermi surface is tangent to the nodal line of the energy gap, resulting in no sign change of the order parameter along the Fermi surface. To more intuitively illustrate this point, Fig. S1 presents the Fermi surfaces in the normal state for different chemical potentials  $\mu$ , along with the corresponding nodal lines of the energy gap when  $\Delta_s = \Delta_s^c(\mu)$ . As observed in the figure, the nodal lines of the energy gap intersect with the Fermi surface at the boundaries of the Brillouin zone, ensuring that there is no sign change of the energy gap across the entire normal state Fermi surface.

## S-2. IMPURITY EFFECT OF BILAYER $\text{La}_3\text{Ni}_2\text{O}_7$ SUPERCONDUCTORS WITH INTERLAYER PAIRING

We investigate the single impurity effect in nickelate superconductors with interlayer  $s$ -wave pairing. The Hamiltonian can be written as  $H_{Ni} = \sum_{\mathbf{k}} \Psi_{\mathbf{k}}^\dagger H_{Ni}(\mathbf{k}) \Psi_{\mathbf{k}}$ .  $H_{Ni}(\mathbf{k})$  is an  $8 \times 8$  matrix expressed as

$$H_{Ni}(\mathbf{k}) = \begin{pmatrix} H_t(\mathbf{k}) & H_\Delta(\mathbf{k}) \\ H_\Delta^\dagger(\mathbf{k}) & -H_t(\mathbf{k}) \end{pmatrix}. \quad (\text{S1})$$

$H_t$  is the tight-binding Hamiltonian,

$$H_t(\mathbf{k}) = \begin{pmatrix} H_A(\mathbf{k}) & H_{AB}(\mathbf{k}) \\ H_{AB}(\mathbf{k}) & H_A(\mathbf{k}) \end{pmatrix}, \quad (\text{S2})$$

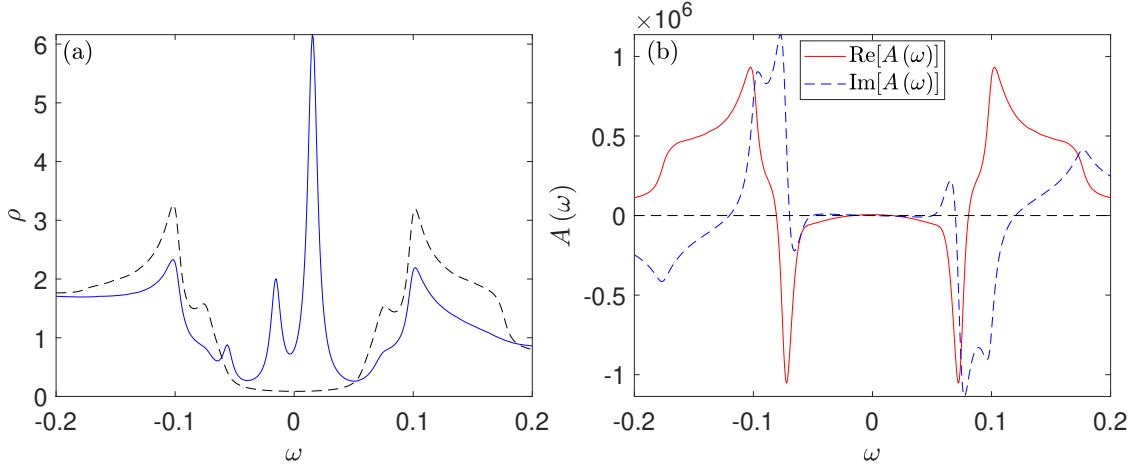


FIG. S2. (a) Solid line: LDOS spectrum at the nearest neighbor site of the impurity site for the nickelate superconductors with interlayer pairing scenario. The dashed line represents the bare LDOS spectrum in the absence of the impurity. (b) Real and imaginary components of the function  $A(\omega)$  for the interlayer pairing.

where

$$H_A(\mathbf{k}) = \begin{pmatrix} T_{xk} & V_k \\ V_k & T_{zk} \end{pmatrix}, H_{AB}(\mathbf{k}) = \begin{pmatrix} t_{x\perp} & V'_k \\ V'_k & t_{z\perp} \end{pmatrix}. \quad (\text{S3})$$

Here

$$T_{xk} = 2t_{1x}(\cos \mathbf{k}_x + \cos \mathbf{k}_y) + 4t_{2x} \cos \mathbf{k}_x \cos \mathbf{k}_y + \epsilon_x \quad (\text{S4})$$

$$T_{zk} = 2t_{1z}(\cos \mathbf{k}_x + \cos \mathbf{k}_y) + 4t_{2z} \cos \mathbf{k}_x \cos \mathbf{k}_y + \epsilon_z \quad (\text{S5})$$

$$V_k = 2t_{3xz}(\cos \mathbf{k}_x - \cos \mathbf{k}_y) \quad (\text{S6})$$

$$V'_k = 2t_{4xz}(\cos \mathbf{k}_x - \cos \mathbf{k}_y) \quad (\text{S7})$$

The tight-binding parameters are referenced in [22].

$H_\Delta$  is the superconducting pairing order part of Hamiltonian, which can be expressed as

$$H_\Delta(\mathbf{k}) = \begin{pmatrix} 0 & 0 & \Delta_{x\perp} & 0 \\ 0 & 0 & 0 & \Delta_{z\perp} \\ \Delta_{x\perp} & 0 & 0 & 0 \\ 0 & \Delta_{z\perp} & 0 & 0 \end{pmatrix}, \quad (\text{S8})$$

The base vector is  $\Psi_k^\dagger = (c_{\mathbf{k}1x\uparrow}^\dagger, c_{\mathbf{k}1z\uparrow}^\dagger, c_{\mathbf{k}2x\uparrow}^\dagger, c_{\mathbf{k}2z\uparrow}^\dagger, c_{\mathbf{k}1x\downarrow}, c_{\mathbf{k}1z\downarrow}, c_{\mathbf{k}2x\downarrow}, c_{\mathbf{k}2z\downarrow})$ . Here the subscripts 1, 2 represent the layer and the subscripts  $x, z$  represent the orbital.

The interlayer superconducting order parameters are determined self-consistently as

$$\Delta_{x/z\perp} = \frac{V}{2N} \sum_{n\mathbf{k}} u_{x/z, n\mathbf{k}}^* v_{x/z, n\mathbf{k}} \tanh \frac{\beta E_{n\mathbf{k}}}{2}. \quad (\text{S9})$$

We use the T-matrix method to investigate the impact of a single impurity, as detailed in Eqs. (3-6) of the main text. Fig. S2(a) displays the numerical results for the local density of states (LDOS) spectra. In Fig. S2(b), we plot the real and imaginary parts of the function  $A(\omega)$  as a function of  $\omega$ . It is observed that the presence of an impurity induces two distinct resonant peaks, symmetrically positioned around the Fermi energy. The emergence of these resonant peaks aligns with the pole condition of the T-matrix. As depicted in Fig. S2(b), both the real and imaginary components of  $A(\omega)$  approach zero at low energies. These findings are qualitatively in agreement with the results from the simplified bilayer model that accounts for interlayer pairing, as discussed in Sec. IV of the main text.